Atmos. Meas. Tech. Discuss., 8, 11853–11891, 2015
www.atmos-meas-tech-discuss.net/8/11853/2015/
doi:10.5194/amtd-8-11853-2015

Atmospheric Measurement Techniques Discussions

A sensitivity study on the retrieval of aerosol vertical profiles using the oxygen A-band

S. F. Colosimo[1], **V. Natraj**[2], **S. P. Sander**[2], **and J. Stutz**[1]

[1]Department of Atmospheric and Oceanic Sciences, UCLA, Los Angeles, CA, USA
[2]Jet Propulsion Laboratory, Caltech, Pasadena, CA, USA

Received: 1 September 2015 – Accepted: 12 October 2015 – Published: 16 November 2015

Correspondence to: S. F. Colosimo (fedele@atmos.ucla.edu)

Published by Copernicus Publications on behalf of the European Geosciences Union.

Abstract

Atmospheric absorption in the O_2 A-band (12 950–13 200 cm^{-1}) offers a unique opportunity to retrieve aerosol extinction profiles from space-borne measurements due to the large dynamic range of optical thickness in that spectral region. Absorptions in strong O_2 lines are saturated; therefore, any radiance measured in these lines originates from scattering in the upper part of the atmosphere. Outside of O_2 lines, or in weak lines, the atmospheric column absorption is small, and light penetrates to lower atmospheric layers, allowing for the quantification of aerosols and other scatterers near the surface.

While the principle of aerosol profile retrieval using O_2 A-band absorption from space is well known, a thorough quantification of the information content, i.e., the amount of vertical profile information that can be obtained, and the dependence of the information content on the spectral resolution of the measurements, has not been thoroughly conducted. Here, we use the linearized vector radiative transfer model VLIDORT to perform spectrally resolved simulations of atmospheric radiation in the O_2 A-band in the presence of aerosol for four different generic scenarios: Urban, Highly polluted, Elevated layer, and Marine–Arctic. The high-resolution radiances emerging from the top of the atmosphere are degraded to different spectral resolutions, simulating spectrometers with different resolving powers. We use optimal estimation theory to quantify the information content in the aerosol profile retrieval with respect to different aerosol parameters and instrument spectral resolutions.

The simulations show that better spectral resolution generally leads to an increase in the total amount of information that can be retrieved, with the number of degrees of freedom (DoF) varying between 0.34–2.11 at low resolution (5 cm^{-1}) to 3.43–5.92 at high resolution (0.05 cm^{-1}) for the four different cases. A particularly strong improvement was found in the retrieval of tropospheric aerosol extinction profiles in the lowest 5 km of the atmosphere. At high spectral resolutions (0.05 cm^{-1}), 1.18–1.7 and 1.31–2.34 DoF can be obtained in the lower (0–2 km) and middle (2–5 km) troposphere, respectively, for the different cases. Consequently a separation of lower and mid tropo-

AMTD
8, 11853–11891, 2015

spheric aerosols is possible, implying the feasibility of identification of elevated biomass burning aerosol plumes (Elevated layer scenario). We find that higher single scattering albedo (SSA) allows for the retrieval of more aerosol information. However, the dependence on SSA is weaker at higher spectral resolutions. The Marine (surface albedo 0.05) and Arctic (surface albedo 0.9) cases show that the dependence of DoF on the surface albedo decreases with higher resolution. While at low resolution ($5\,cm^{-1}$) the DoF is 1 for the Marine case and 0.34 for the Arctic case, the DoF considerably increase at $0.05\,cm^{-1}$ resolution to 3.8 and 3.4, respectively. In the Arctic case this is an improvement of a factor of 10. The simulations also reveal a moderate dependence of information content on the integration time of the measurements, i.e., the noise of the spectra. However, our results indicate that a larger increase in DoF is obtained by an increase in spectral resolution despite lower signal-to-noise ratios.

1 Introduction

Atmospheric aerosols play a central role in the Earth's radiative budget. Together with various greenhouse gases, aerosols represent the most significant anthropogenic forcers responsible for climate change. However, uncertainties about the origin and composition of aerosol particles, their size distribution, concentration, spatial and temporal variability, make climate change prediction challenging. In order to quantify the influence of aerosols on the Earth's climate and to better validate climate models, information about their global abundance, properties and height distribution are needed.

Aerosol vertical and horizontal distribution significantly affects total radiative forcing in the Earth's troposphere and stratosphere. Aerosol particles transported by wind over long distances in the free troposphere affect climate on larger spatial scales than aerosols close to the surface, e.g. those confined in the Boundary Layer, have shorter lifetimes and have a more local impact on climate and air quality. Hence, knowledge of the vertical and horizontal distribution is crucial to understanding the impact of aerosols (Geddes and Bösch, 2015; Koffi et al., 2012; Vuolo et al., 2014; Samset et al., 2013;

AMTD
8, 11853–11891, 2015

Zarzycki and Bond, 2010). Similarly, the climate impact through indirect effects, e.g., aerosol altering cloud microphysical properties, also depends strongly on the altitude of the aerosol (Hansen and Lacis, 1990).

To fully understand the impact of aerosols on a global scale, the use of passive satellite remote sensing observations has been shown to be especially useful. Algorithms for aerosol and cloud retrieval, e.g. over land (Sanders et al., 2015; Kalashnikova et al., 2013; Diner et al., 2012; Martonchik et al., 2009) using MISR (Multi-angle Imaging SpectroRadiometer) data (Diner et al., 1989), and over the ocean (Sanders et al., 2015; Dubuisson et al., 2009; Duforêt et al., 2007) using the POLDER (Polarization and Directionality of the Earth's Reflectances) (Deschamps et al., 1994) and MERIS (Medium Resolution Imaging Spectrometer) (Rast et al., 1999) data, have been successfully developed in the last decade. Many of these instruments include a window around the spectrally unresolved O_2 A-band.

Investigations on the absorption and continuum part of the oxygen A-band (Fischer and Grassl, 1991; Gabella et al., 1999; Heidinger and Stephens, 2000; Rozanov and Kokhanovsky, 2004; Natraj et al., 2005; Boesche et al., 2008) have shown how satellite measurements can be used to retrieve aerosol and cloud properties.

Multispectral high-resolution radiance and polarization measurements in the absorption spectrum of molecular O_2 have been successfully used to retrieve the vertical distribution of aerosols and clouds (Geddes and Bösch, 2015; Hollstein and Fischer, 2014; Sanders and de Haan, 2013; Sanghavi et al., 2012; Kokhanovsky and Rozanov, 2010; Hasekamp and Landgraf, 2007).

O_2 A-band data from the SCIAMACHY (Scanning Imaging Absorption Spectrometer for Atmospheric Chartography) (Bovensmann et al., 1999) instrument has shown that the retrieval of aerosol vertical distribution depends strongly on aerosol optical properties (single scattering albedo and phase function in primis) and surface parameters (Corradini and Cervino, 2006).

Natraj et al. (2007) demonstrated that neglecting polarization in the forward modeling of O_2 A-band backscatter measurements from space-based instruments, can af-

AMTD
8, 11853–11891, 2015

fect the retrieval precision in different ways for different atmospheric scenarios. They investigated errors resulting from ignoring polarization in retrievals for varying geometry, surface reflectance and aerosol loading, using simulated OCO (Orbiting Carbon Observatory) (Crisp et al., 2004) data.

Frankenberg et al. (2012) showed that the information content for both aerosols and trace gases can be improved by adding off-nadir viewing angles in hyperspectral measurements. They also investigated the dependence of the aerosol information content for different instrument specifications in multi-angle retrievals. Further, over vegetated areas, chlorophyll fluorescence provides an additional contribution to the signal in the oxygen A-band (Sanders and de Haan, 2013). Investigation of this phenomenon (Frankenberg et al., 2011) demonstrates that the signal from atmospheric scattering is affected by this type of emission, and that neglecting it can cause systematic biases in the retrieval of aerosol parameters such as layer height and optical thickness, or surface properties such as surface pressure and albedo.

Sanghavi et al. (2012) used a combination of oxygen A- and B-band SCIAMACHY data to infer a complete vertical distribution of aerosols for a specific area in Kanpur (India). Recently, Geddes and Bösch (2015) pointed out that the height and optical depth of aerosol layers can be properly retrieved from satellites using the O_2 A-band only if the layers are close to the free troposphere. Their study shows that, while satellite observations can provide good information on aerosol plumes close to the free troposphere, information on Boundary Layer aerosols is still limited. A concept study by Hollstein and Fischer (2014), investigated the role of instrument spectral resolution and noise on aerosol profile retrievals from O_2 A-band measurements, using a forward operator based on look-up tables. They varied instrument resolution, signal-to-noise ratio, and spectral sampling, and performed optical depth and layer height retrievals for different aerosol types. Their results indicate that the retrieval generally benefits from improved spectral resolution, and strongly depends on the signal-to-noise level.

The aim of this work is to evaluate the amount of vertical information on aerosol extinction profiles that can be extracted from satellite-based remote sensing measure-

AMTD
8, 11853–11891, 2015

ments of the O_2 A-band. Of particular interest is the impact of improvements in spectral resolution on the aerosol profile information content. To this end, we perform simulations of high resolution O_2 A-band spectra as observed by a satellite instrument, and use optimal estimation theory to determine the amount of vertical information with respect to aerosol profile retrievals, and its dependence on spectral resolution and noise. Since our primary focus is the amount of aerosol information, we do not consider the effect of chlorophyll fluorescence in this work. Methods to quantify the chlorophyll fluorescence have been developed (Frankenberg et al., 2011), and we assume that its contribution can be independently assessed and corrected. By performing a detailed calculation and comparison of the information content retrieval for different altitude ranges (as opposed to the total columnar value that is typically reported), we investigate, for a variety of scenarios, if the tropospheric information can be isolated and evaluated.

The paper is organized as follows: Sect. 2 provides an overview of the atmospheric model and the a priori assumptions, along with a description of the radiative transfer (RT) calculation and the convolution for different instrument specifications. A description of the signal-to-noise model is also given for a better understanding of the results. Section 3 describes the theory behind the information content analysis and defines the quantities involved in the determination of the various retrieval metrics. Section 4 explains how the information content tests were performed, and compares the results for the different cases. Section 5 presents some concluding remarks.

2 Radiative transfer simulations

In order to test the sensitivity of different instrument specifications to aerosol retrievals, high resolution O_2 A-band spectra simulated with a RT model (described below) were convolved with Gaussian instrument functions of different spectral resolutions. To investigate the effects of noise, we used modeled radiances, assumptions on the instrument response, and different integration times. These calculations were performed for

AMTD
8, 11853–11891, 2015

different a priori aerosol profiles and covariances. This section will describe the RT calculation and the convolution.

2.1 Atmospheric model

The interpretation of remotely sensed data often requires radiative transfer models (RTMs) to simulate radiances and their analytic derivatives (Jacobians) with respect to various atmospheric and surface parameters. A variety of RTMs have been developed over the years. Our choice of RTM was guided by the need to perform a very large number of calculations to fully resolve the O_2 A-band, provide an accurate description of the full Stokes vector, and have the ability to effectively calculate Jacobians with respect to various atmospheric parameters. With the above needs in mind, we chose VLIDORT as the RTM (Spurr, 2006). The VLIDORT model calculates all of the Stokes parameters in a multi-layer, multiple scattering medium. The model is also fully linearized; the advantage of this design is that an entire set of intensities and weighting functions required for an iteration step in a multi-parameter atmospheric retrieval can be generated simultaneously and in an analytic fashion, with a single call to the model, saving a significant amount of computing time. This feature makes the code ideally suited to retrieval applications, where computational time and memory requirements may represent a problem. A complete kernel-model Bidirectional Reflectance Distribution Function/Matrix (BRDF/M) set is also implemented for surface reflection and surface property weighting functions, including surface thermal emission (isotropic). VLIDORT is not internally linked with any databases for spectral optical properties and/or precomputed look-up tables. The code uses a user-defined environment, where geophysical atmospheric inputs such as vertical profiles (thermal, trace gases and aerosol), optical parameters (single scattering albedo, asymmetry parameter, optical thickness, phase function moments) or spectral properties (cross sections, wavelengths), depend on the specific application and need to be defined by the user.

For this study, the atmosphere is divided into 60 layers, with a pressure range between 1001.6 mbar (surface) and 0.3 mbar (top of the atmosphere) and an altitude

AMTD
8, 11853–11891, 2015

range between 0 and 55 km. Vertical temperature and pressure profiles were based on the U.S. Standard Atmosphere (NOAA, 1976) after an interpolation to a customized altitude grid. The vertical grid spacing has been set to 0.2 km in the 0–5 km range, 0.5 km in the 5–10 km range, and 1 km above 10 km altitude. The temperature, pressure, molecular, and aerosol properties are considered homogeneous within each layer. Molecular oxygen is the only absorber considered in his study. O_2 spectral line parameters were taken from the HITRAN 2008 database (Rothman et al., 2009). Clouds were not considered and scattering is assumed to be caused by molecules and aerosols only. A Lambertian reflecting surface is assumed, with a surface albedo $a = [0.05, 0.1, 0.9]$, depending on the type of simulated atmospheric scenario. For a realistic satellite observation geometry, we assume a constant solar zenith angle of 45°, and an instrument looking down at 30° off-nadir.

In this study, we consider four aerosol profiles, each representative of a different atmospheric scenario, to cover a variety of atmospheric/surface conditions (Fig. 1):

- *Urban*: the urban profile reflects typical conditions in a moderately polluted urban or rural atmosphere, where high levels of aerosol are constrained to a well define Boundary Layer (BL) (Schafer et al., 2014; Baidair et al., 2013). The aerosol profile is thus constructed assuming a constant a priori aerosol extinction coefficient $k_{ext} = 0.2\,km^{-1}$ below a fixed Boundary Layer Height (BLH) of 1 km. Above the BL, extinction decreases exponentially with altitude (Wagner et al., 2011). A value of $a = 0.1$ for the surface albedo has been adopted for this test case.

- *Highly polluted*: for highly polluted urban areas the vertical profile shape is similar to that of the urban case, but the aerosol extinction in the Boundary Layer is higher (Clemer et al., 2010). We thus use the same parameterization as in the urban case, but with a larger extinction coefficient $k_{ext} = 1.0\,km^{-1}$ below a BLH of 1 km.

AMTD
8, 11853–11891, 2015

– *Elevated layer*: we also considered a typical biomass burning plume to test the detection of aerosol layers in the free troposphere (Pelon et al., 2008; Johnson et al., 2008; Wandinger et al., 2002; Ansmann et al., 2000; Anderson et al., 1996; Matsui et al., 2010). The profile is confined to a layer between 2 and 4 km altitude with constant $k_{ext} = 0.2\,km^{-1}$. BL aerosol extinction and height are set to $k_{ext} = 0.1\,km^{-1}$ and 0.4 km, respectively. Surface albedo is set to $a = 0.1$.

– *Marine–Arctic*: we also investigated a Marine–Arctic case with lower aerosol extinction at the surface and a lower Boundary Layer. The Arctic case is representative of an environment with pollution, often referred to as "arctic haze" (Shaw, 1995). We assume the same k_{ext} and BLH for both cases to simulate the aerosol profile, changing the surface albedo in the respective environment. Many studies have shown the great variability of extinction and BLH of aerosol in these two environments (Tesche et al., 2014; Sayer et al., 2012; Frieß et al., 2011; Yu et al., 2010; Li et al., 2006; Yamanouchi et al., 2005; Quinn et al., 2002; Leiterer et al., 1997; Blanchet and List, 1983). Consequently, these profiles are only meant to be representative of typical conditions. For both profiles we adopted a constant value of $k_{ext} = 0.05\,km^{-1}$ (above the BL, extinction decreases exponentially with altitude) and a value of 0.4 km for BLH. In this case, surface albedo values of $a = 0.05$ and $a = 0.9$ have been adopted for the Marine and a snow-covered Arctic scenario respectively.

It is worth mentioning that the adopted extinction profiles are not representative of any particular area or location on Earth. They only represent a plausible parameterization for the different scenarios. Figure 1 shows the vertical profiles for all cases. A set of four single scattering albedos $\omega = [0.8, 0.85, 0.9, 0.95]$, together with an asymmetry parameter $g = 0.7$, were used for this test to describe the optical properties of the aerosol in the different cases (Baidair et al., 2013; Clemer et al., 2010; Xia et al., 2006; Dubovik et al., 2002; Quinn et al., 2002).

AMTD
8, 11853–11891, 2015

2.2 High resolution spectra and convolution

VLIDORT was used to generate oxygen A-band high resolution radiance spectra $L_h(\nu_0)$ in the spectral range $\Delta = 12\,950$–$13\,200\,\mathrm{cm}^{-1}$ (757–772 nm), with a fixed spectral sampling $\Delta\nu_0 = 0.002\,\mathrm{cm}^{-1}$ and a number of points given by $\nu_0 = \Delta/\Delta\nu_0 = 125\,000$. At this high resolution all spectral features of the oxygen A-band are fully resolved.

To simulate the measurement of the O_2 A-band by a space-borne spectrometer, Gaussian instrument response functions for different Full Widths at Half Maximum (FWHM) were calculated. The high resolution O_2 spectra were then convolved with this function. The convolved spectrum was then down-sampled by integrating the radiances over a grid point of width $\Delta\nu$. We chose to keep the ratio of FWHM to $\Delta\nu$ constant at 5, to avoid under or oversampling of the spectrum during the convolution. Therefore, when we increased the instrument resolution (decreasing FWHM), we decreased $\Delta\nu$ accordingly:

$$\frac{\mathrm{FWHM}}{\Delta\nu} = 5 \tag{1}$$

The Gaussian function representing the instrumental response is described as:

$$G(\nu', \mathrm{FWHM}) = \frac{1}{\sigma\sqrt{2\pi}} \cdot \exp\left[-\frac{\nu'^2}{2\sigma^2}\right] \tag{2}$$

with σ defined as

$$\sigma = \frac{\mathrm{FWHM}}{2\sqrt{2\ln 2}} \tag{3}$$

where the first factor in Eq. (2) takes into account the normalization of the area of the function $G(\nu', \mathrm{FWHM})$ to 1, and ν' represents the Gaussian spectral sampling extended to ±5 FWHM for each spectral channel.

AMTD
8, 11853–11891, 2015

The spectral radiance used for this study is the result of the convolution of the simulated high resolution radiance with the instrument spectral response function (each channel is assumed to be independent of the others). The convolved radiance L_c is expressed as:

$$L_c(\nu) = \sum_{\nu'} L_h(\nu')\, G(\nu' - \nu)\, \Delta\nu \tag{4}$$

calculated as the sum over the instrument response function spectral sampling ν', of the product of the spectral response function and the high resolution radiance L_h, expressed over the set of frequencies ν'. The index $\nu = \Delta/\Delta\nu$ for each instrument channel represents the chosen sampling grid covering the entire spectral range Δ. Figure 2 shows an example of the high resolution spectrum ($\Delta\nu_0 = 0.002\,\mathrm{cm}^{-1}$) convolved with different instrument function FWHM.

2.3 Noise model

The instrument noise model assumes that measurement noise is dominated by photon shot noise. Shot noise comes from the statistical uncertainty of the number of photons sampled by the detector, which can be described by a Poisson distribution. This assumption is quite accurate for modern spectrometers. Based on Poisson statistics we calculate the standard deviation of the radiance measurement σ_m as follows:

$$\sigma_m = \sqrt{N} \tag{5}$$

with relative signal-to-noise ratio (SNR) proportional to the square root of the number of photons N:

$$\mathrm{SNR} = \frac{N}{\sigma_m} = \sqrt{N} \tag{6}$$

AMTD
8, 11853–11891, 2015

The measurement error is thus proportional to the standard deviation σ_m (which can be calculated as the square root of N) with a relative variance σ_m^2. To calculate the number of photons N falling on the detector, we use the following expression:

$$N = \frac{L_c(\nu) \cdot \Delta t \cdot \epsilon \cdot \Omega \cdot A}{E_{ph} \cdot \Delta \nu} \quad (7)$$

where E_{ph} is the energy of a photon at 13 150 cm^{-1} (760 nm), Δt is the integration time, ϵ is the efficiency of the spectrometer/detector combination, Ω is the solid angle of the field of view of the instrument and A is the slit surface area. For our calculations we use $E_{ph} = 2.6 \times 10^{-19}$ J photon^{-1}, $\epsilon = 0.05$, $\Omega = 0.01$ steradians, $A = 5.0 \times 10^{-7}$ m^2.

We implemented this noise model without considering any particular design or instrument specifications. Signal-to-noise ratios (SNR) outside of the A-band, i.e. at 13 190 cm^{-1}, for a $\Delta t = 1$ s varies from 5000 at the lowest resolution to 500 at the highest resolution. These SNR values are somewhat higher than those of current satellite instruments, but in the range of high quality future instruments. We also analyze the sensitivity of our simulations to noise by varying the integration time between 0.1 and 5 s. The sensitivity of the model to the radiance level (which depends on resolution), and to the integration time, allows us to evaluate the capability of different sensors to retrieve information for different aerosol scenarios.

3 Information content analysis

To determine the information content of an aerosol retrieval based on the spectroscopic observations in the O_2 A-band at different resolutions, we use an optimal estimation formalism, as described in detail in Rodgers (Rodgers, 2000). According to the Bayesian formalism, the sensitivity of the retrieval of a set of parameters, to the measurement, is expressed by the so-called *gain matrix* **G**:

$$\mathbf{G} = (\mathbf{K}^T \mathbf{S}_\epsilon^{-1} \mathbf{K} + \mathbf{S}_a^{-1})^{-1} \mathbf{K}^T \mathbf{S}_\epsilon^{-1} \quad (8)$$

AMTD
8, 11853–11891, 2015

where **K** is the functional derivative matrix, also called Jacobian, which represents the change in the measurement for a unit change in the retrieved parameter. VLIDORT provides analytic derivatives of the Stokes vector field with respect to any atmospheric or surface property (Spurr, 2006). The Jacobians required in Eq. (8) can be calculated from these weighting functions by application of the chain rule.

An important part of optimal estimation analysis is the covariance matrix, $\mathbf{S}_a$, which quantifies the knowledge of the retrieved parameter prior to the measurement, and the measurement error covariance matrix, $\mathbf{S}_\epsilon$, which quantifies the error of the measurement. We calculate $\mathbf{S}_\epsilon$ according to the instrument noise model described in Eqs. (5)–(7). We will discuss the choice of $\mathbf{S}_a$ further below. We assume both matrices to be diagonal, with all the off-diagonal elements equal to zero. Every element of the diagonal thus represents the variance of the respective element in the a priori parameter and the measurement vector, respectively. We assume the errors to be uncorrelated.

The sensitivity of the retrieval to the true state of the parameter is expressed by the so called *Averaging Kernel* (AK) matrix **A**:

$$\mathbf{A} = \mathbf{GK} \tag{9}$$

which is equal to a unit matrix for an ideal retrieval, when a perfect match between the a priori and the retrieved parameter is achieved. The trace of **A** represents the number of Degrees Of Freedom (DoF), which represent the total number of independent pieces of information derived by the retrieval. Combining Eqs. (9) and (8), the averaging kernel matrix **A** can be written as:

$$\mathbf{A} = (\mathbf{K}^T\mathbf{S}_\epsilon^{-1}\mathbf{K} + \mathbf{S}_a^{-1})^{-1}\mathbf{K}^T\mathbf{S}_\epsilon^{-1}\mathbf{K} \tag{10}$$

which shows the dependence of DoF on the $\mathbf{S}_a$, $\mathbf{S}_\epsilon$ and **K** matrices.

The AK can be seen as a linear representation of the information content of the retrieval parameters. It represents the relationship of the retrieval to the true state vector, and ranges between 0 and 1. An AK close to 1 means that a near-perfect agreement between the retrieved parameter and the true state has been reached. As it represents

AMTD
8, 11853–11891, 2015

an indication of what the measurement is sensitive to, the AK can also be interpreted as the vertical resolution of the retrieval, because it provides important information on the vertical sensitivity of the instrument, with its maximum corresponding to the range of altitudes where the maximum sensitivity occurs.

A sample AK is shown in Fig. 3, where four different regions of the atmosphere are color coded. In this case, the region between 2 and 5 km represents the altitude range with the highest sensitivity to aerosol extinction.

Based on this formalism we perform two different sensitivity studies. In the first, we study the effect of instrument resolution by varying FWHM and $\Delta\nu$ (Eq. 1), and scale the relative noise σ_m according to the radiances at the various spectral resolutions, i.e. at higher spectral resolution fewer photons are sampled per channel, resulting in larger relative errors and vice versa. It should be noted that the number of channels also varies in this test, as discussed above. In the second test, we keep the instrument resolution constant and only vary the relative noise by changing the integration time Δt in Eq. (7). This calculation serves to better understand the contribution of the change in per-channel noise with resolution to the information content.

We thus investigate the dependence of the degrees of freedom of the retrieved aerosol extinction profile on different instrument spectral resolution FWHM (and relative spectral binning $\Delta\nu$) and different integration time Δt. We perform both tests for different a priori aerosol extinction profile errors, expressed through the $\mathbf{S}_a$ matrix in Eq. (8), to investigate the influence of prior knowledge of the aerosol extinction. We assume that the diagonal elements of $\mathbf{S}_a$, which represent the a priori extinction profile variances for every single layer, are constant at all altitudes.

Six different a priori variances are used: 0.7, 0.5, 0.2, 0.1, 0.05, 0.01, which correspond to a relative error of 83.7, 70.7, 44.7, 31.6, 22.4 and 10.0 % of the a priori aerosol extinction profile, respectively. It should be noted that performing this sensitivity calculation is very important, as the total pieces of information of a system strongly depend on the a priori knowledge of the retrieval parameter, as we will discuss in the following section.

AMTD
8, 11853–11891, 2015

4 Results and discussion

4.1 Resolution sensitivity

In order to understand the impact of different instrument resolutions on the total amount of information available, we perform calculations for five pairs of values of FWHM and $\Delta\nu$: FWHM = (5, 1, 0.5, 0.1, 0.05) cm^{-1} and $\Delta\nu$ = (1, 0.2, 0.1, 0.02, 0.01) cm^{-1}. Tables showing the numerical values of the DoF for the complete set of resolutions can be found in the Supplement.

Using the relationships previously described, we calculate the total DoF for every pair of these values. All DoF values are calculated for the spectral range of 13 122–13 140 cm^{-1}. An integration time of Δt = 1 s has been used for the tests.

The a priori knowledge of the aerosol profile is defined by the covariance matrices $\mathbf{S}_a$. As a first test, we investigate the effect of different $\mathbf{S}_a$ on the total DoF for the Urban aerosol scenario, with $\omega = 0.85$ and a nadir looking geometry. Figure 4a shows that increasing the resolution increases the amount of information available for the aerosol extinction profile retrieval. This is true for every a priori value of the diagonal elements of $\mathbf{S}_a$, i.e. the a priori aerosol extinction profile relative errors.

A two orders of magnitude change in the resolution (i.e., FWHM from 5 to 0.05 cm^{-1}) leads to a three times (or more) increase in the DoF for all of the covariance values, showing the importance of fully resolving the narrow features of the band. On the other hand, the DoF decreases as the a priori knowledge (smaller relative error) of the retrieval parameter increases. This is due to the nature of optimal estimation: a better a priori knowledge of the parameter to be retrieved reduces the amount of extra information that can be obtained from the measurement.

While the extreme values of $\mathbf{S}_a$ (aerosol relative errors of 83.7 and 10.0 % respectively) are not very realistic, we implement them in this test to take into account a wider set of possible aerosol conditions. For the rest of the tests, we choose a fixed value

AMTD
8, 11853–11891, 2015

of $\mathbf{S}_a = 0.2$ (44.7 % relative error), which represents a reasonable choice of average aerosol uncertainties for the different profiles.

We also analyze the impact of different single scattering albedos on the DoF for the Urban scenario (Fig. 4b). At low spectral resolutions the DoF increases with an increase in ω. This is due to the larger scattered radiance from the aerosol at higher ω, which increases the signal, as well as the contrast to the surface. The DoF increase from a ω of 0.8 to 0.95 is a factor of 1.76 at low resolution. The DoF also increases with resolution (lower values of $\Delta\nu$ and FWHM) for all ω. Interestingly, however, the effect of the single scattering albedo is much reduced at higher spectral resolutions. The DoF improvement from a ω of 0.8 to 0.95 is only a factor of 1.25. It thus appears that resolving spectral features decreases the dependence of the retrieval on ω. This reduction is likely due to the fact that the retrieval at high spectral resolution extracts information based on the O_2 band shape, rather than the radiances alone.

For the rest of this study we will use $\omega = 0.95$ and a 30° off-nadir instrument viewing geometry. It should be noted that increasing ω further does not considerably change the results of the tests, as can already be seen in Fig. 4b, where the dependence of DoF on ω decreases with increasing ω. With the values of ω and $\mathbf{S}_a$ fixed we can now analyze the dependence of the DoF on spectral resolution for the various aerosol profiles (Fig. 5a).

In the urban and highly polluted scenarios the DoF increases from a value of approximately 2 at 5 cm^{-1} resolution to 5.4–5.9 at 0.05 cm^{-1} resolution. The DoF improvement with spectral resolution of 2.7 (Urban) and 2.8 (Highly polluted) is very similar for both scenarios. The highly polluted scenario has, in general, a 5–10 % higher DoF due to its five times higher BL aerosol extinction. The DoF change is surprisingly small, considering the large change in aerosol extinction; our results thus seem to be applicable for a wide range of polluted urban scenarios.

The DoF for the Elevated layer scenario are somewhat smaller than those in the urban polluted scenarios, changing from 1.4 to 4.6 as the resolution varies from 5 to 0.05 cm^{-1}. The change in resolution for an aerosol layer between 2 and 4 km provides

AMTD
8, 11853–11891, 2015

an improvement in the DoF of a factor of 3.3. It is evident that resolution has a stronger impact on DoF for the Elevated layer scenario than for the urban polluted scenario.

In the Marine scenario the DoF are lower than in the previous cases, due to the generally lower aerosol extinction. At low resolutions only 1.2 pieces of information can be retrieved. Again, a resolution of 0.05 cm^{-1} leads to an improvement in the DoF of a factor of 3.2, yielding a DoF of 3.8. As the aerosol extinction profile used is the same in the Marine and Arctic scenarios, the difference in DoF between these scenarios can be attributed to a surface albedo effect. The higher albedo in the Arctic case leads to lower DoF, in particular for lower spectral resolutions. In fact, at low resolutions, almost no information (DoF = 0.34) can be retrieved. However, higher spectral resolutions lead to a DoF improvement of a factor of ten, and the DoF at a resolution of 0.05 cm^{-1} is only 10 % lower than in the Marine case. It should be noted that in a test with an albedo of 0.3 (not shown), typical of a vegetated surface (Zhengjia et al., 2015), a similar behavior was observed and the DoF in this case follow the DoF of the Arctic case closely. High spectral resolution thus seems to be crucial for aerosol retrievals over snow.

The poor retrievals at low resolution over snow are due to the well-known problem of distinguishing highly scattering aerosol over a high albedo surface. The lack of contrast makes it impossible for a radiance-based retrieval to determine the aerosol extinction profile or even the column. In the Marine case, where the albedo is 0.05, the total DoF at low resolution is 1.19, indicating that a total atmospheric aerosol optical depth can be retrieved. In the Arctic case, the total DoF is only 0.34, making it impossible to even retrieve a column value. On the other hand, since the retrievals at high spectral resolutions use information from the O_2 absorption band centers and wings, they are partially based on radiances that do not penetrate all the way to the surface. There is, therefore, less sensitivity to surface properties.

4.2 Altitude sensitivity

The total DoF provides information about the total column. On the other hand, the AK matrix contains information related to the atmospheric layers; therefore, a calculation of

AMTD
8, 11853–11891, 2015

subsets of the matrix **A** (and hence subsets of the Trace[**A**] = DoF) allows for an evaluation of the DoF, and its dependence on spectral resolution, for different altitude ranges. In order to get a better understanding of the altitude with maximum amount of information for the different scenarios, we divide the atmosphere in four altitude regions: I = [0–2] km, II = [2–5] km, III = [5–15] km, IV = [15–50] km, i.e. I and II for the lower and mid-troposphere, III for the upper troposphere/lower stratosphere, and IV for the stratosphere. Figure 3 shows the color coded AK for the four regions for a generic simulation. The results of the altitude-resolved DoF, and its dependence on spectral resolution for the different scenarios are reported in Fig. 5b–f. In all scenarios, an improvement in the DoF in the different altitude intervals is observed. This follows the general trend already observed in the whole-atmosphere DoF. However, the improvement of information with improving spectral resolution is not uniform with altitude.

In the urban and highly polluted scenarios (panel (b) and (c) respectively), the stratospheric DoF increases from 0.8 and 0.6 to 1.19 and 1.07, respectively, as the spectral resolution increases from 0.5 to a 0.05 cm^{-1}. This change in DoF is smaller than that observed in the lower and mid-troposphere, where the increase is a factor of 4.1 and 3, respectively. In fact, for both regions, the DoF is below 1 for the low-resolution case and increases to values of 1.5–2.5 for the high resolution case. Both scenarios require at least a resolution of FWHM = 0.1 cm^{-1} to reach a DoF greater than 1 in the lower and mid-troposphere. It is evident that a high spectral resolution is crucial for tropospheric aerosol extinction retrievals. At high resolution (FWHM = 0.05 cm^{-1}), almost 64 % (urban) and 68 % (highly polluted) of the total DoF comes from Regions I and II.

The impact of spectral resolution on tropospheric aerosol retrievals is even more obvious in the Elevated layer scenario. In this case a resolution of FWHM = 0.05 cm^{-1} is required to reach a DoF greater than 1 in Regions I and II (panel (d)). At this resolution, almost 60 % of the total DoF originates from the lowest 5 km of the atmosphere with a DoF of 2.7 in this region (sum of DoF in region I and II). The improvement in the information content at higher resolutions is even clearer in this scenario, with a factor of 8.5 and 5.6 increase in DoF in Regions I and II, respectively. It should also be noted

AMTD
8, 11853–11891, 2015

that, at higher resolutions, it is possible to retrieve an elevated aerosol layer above the BL (see profile in Fig. 1).

The Marine and Arctic scenario results (panel (e) and (f) respectively) are also in line with the previous tests. A resolution of FWHM = 0.05 cm^{-1} is needed to achieve DoF greater than 1 in the lower and mid-troposphere. The total number of DoF for the tropospheric levels (sum of Regions I and II) at FWHM = 0.05 cm^{-1} resolution is 2.54 (66 % of the total) for the Marine case and 2.49 (72 % of the total) for the Arctic scenario. The improvement in DoF with resolution is most pronounced in the Arctic case, where DoF in Region I and II are below 0.1 and increase by a factor of 59 at high resolution. As in the total DoF analysis, an altitude sensitivity test (not shown) with the same aerosol profile and a surface albedo $a = 0.3$ representative of a vegetated land, follows the altitude resolved DoF of the Arctic case closely, showing the same improvement with increasing spectral resolution.

It is worth mentioning again that the high resolution retrievals substantially reduce the albedo effect of the retrieval. In particular, in the lower and mid-troposphere, there is no difference in the DoF at high resolutions. Again, this implies that the retrieval is dominated by the information in the O_2 absorption bands, and in particular in the band wings, which allow probing different altitudes in the atmosphere without relying on reflected radiances from the surface.

4.3 Integration time sensitivity

Here we analyze the effects of different integration times (i.e. the effect of sampling noise) Δt on DoF, investigating the dependence due to the change in photon noise in two different tests. The first test is a comparison among the same six different a priori aerosol uncertainties used for the resolution test (Fig. 4a), keeping the spectral resolution constant, with fixed values of FWHM = 0.1 cm^{-1} and $\Delta\nu = 0.02\,cm^{-1}$, and with $\omega = 0.95$. The second test is a comparison among the same values of spectral resolutions used for all the previous calculations. In this last test, we keep the a priori aerosol uncertainty fixed to $\mathbf{S}_a = 0.2$ (44.7 % relative error), varying instrumental FWHM to in-

AMTD
8, 11853–11891, 2015

vestigate how photon noise affects the dependence of the content of aerosol information on the resolution. Six different integration times Δt (ranging among 5, 2, 1, 0.5, 0.2 and 0.1 s) have been used for these two tests.

In the first test, the effect of the aerosol uncertainties on the content of information is investigated for different integration times. When the spectral resolution is fixed, Eq. (7) shows that the noise depends only on the variation of the integration time (all the other quantities are fixed). Integration time, however, is related to the covariance matrix $\mathbf{S}_\epsilon$ through its dependence on the measurement noise σ_m (Eq. 5). For a fixed a priori aerosol extinction profile relative error, Eq. (10) shows that the averaging kernel matrix **A** (and hence DoF) depends only on $\mathbf{S}_\epsilon$, because the **K** matrix (representing the variation of the radiance with respect to the retrieved parameter) depends on the spectral resolution, which is fixed for this test.

Figure 6a shows that the DoF increases with increasing Δt for every value of $\mathbf{S}_a$. While the change with integration time seems reasonable, the DoF does not seem to follow the square-root dependence on Δt shown in Eq. (5). For a realistic value of $\mathbf{S}_a = 0.2$, between $\Delta t = 5$ s and $\Delta t = 0.1$ s (50 times smaller), the DoF differ by about 23 %. For a poor knowledge of the aerosol profile (83.7 % relative error) they differ by 21 % while for a good a priori knowledge (10 % relative error) the difference is about 37 %.

The second test (Fig. 6b) shows that resolution is the main driver in aerosol profile retrievals for high resolution measurements. The comparison with different photon noise show the importance of a high resolution vs. integration time. The gain, in terms of content of information when a measurement at high resolution is performed, is greater than any increase due to a change in Δt. A factor of 10 change in the integration time leads to an improvement of about 15 % in the content of information, whereas the same change at high resolution (0.5 to 0.05 cm^{-1}) can lead up to a 43 % increase in the DoF. Since spectral resolution and noise are linked to each other, our results indicate that it advantageous to use higher spectral resolution despite lower SNR.

AMTD
8, 11853–11891, 2015

5 Conclusions

This study investigates the dependence of the information content of aerosol profile retrievals from high spectral resolution radiance measurements in the O_2 A-band. For this purpose, the DoF of the aerosol state vector elements has been derived for different spectral resolutions and sampling intervals. Four different atmospheric scenarios, covering a variety of vertical aerosol extinction profiles and albedos, were considered.

In general, our simulations show that high resolution measurements in the O_2 A-band considerably improve the aerosol profile information content and thereby the retrieval of aerosol profiles.

The following conclusions can be drawn based on our results:

- The retrieval of tropospheric aerosol extinction profiles in the lowest 5 km of the atmosphere is considerably improved at higher spectral resolution. At the highest resolution considered here (0.05 cm^{-1}), the number of pieces of information that can be retrieved varies from 3.5–4 in polluted urban cases, to around 2.5 in cleaner Marine and Arctic cases.

- The high-resolution retrievals have sufficient information content in the mid-troposphere to allow the identification and quantification of the extinction of elevated aerosol layers, such as those from biomass burning. The DoF of 1.27 and 1.46 in the lower and mid-troposphere allow distinction of an aerosol at the surface from that in an Elevated layer.

- The retrieval sensitivity to aerosol single scattering albedo is diminished at a high spectral resolution. The total DoF varies from 4.2 for $\omega = 0.8$, to 5.3 at ω values approaching 1. This is in contrast to the behavior at low resolutions, where the difference is close to a factor of two.

- The influence of surface albedo is considerably reduced at high spectral resolutions, as illustrated by a comparison of a marine and an arctic case with identical

AMTD
8, 11853–11891, 2015

aerosol profiles. This is particularly true for the lower and mid-troposphere where retrievals at high albedos are not possible at low resolutions, while DoF above 1 in the lowest 2 km allow the retrieval of tropospheric aerosol extinction when the resolution is high enough. This is because the high-resolution retrieval is based on the spectroscopic information, i.e. the absorption band shape, rather than continuum radiances.

– Noise considerations indicate that higher-spectral resolution is advantageous for the aerosol total information content despite the lower signal-to-noise ratios. The high dynamic range of optical thickness in the O_2 absorption lines seem to outweigh the noise that is introduced by the high resolution.

The results of this study clearly show how increases in spectral resolution increase the amount of information available. Our results agree with other studies investigating the amount of information available for aerosol retrieval using the O_2 A-band. Investigations on retrieval information content of aerosol over sea and vegetated areas, simulating O_2 A-band SCIAMACHY nadir data at low spectral resolution (FWHM = 0.4 nm or 6.9 cm^{-1}), infer DoF of 3.2 and 2.3 respectively (Corradini and Cervino, 2006). The same study, however, points out that increasing spectral resolution leads to a better vertical resolution accuracy for the retrieval. A value of 4.1 for the DoF is obtained when spectral resolution is increased to 0.05 nm (0.86 cm^{-1}).

Other studies find DoF ranging between 2 and 7, using both nadir and multi-angle simulations for the retrieval process (Frankenberg et al., 2012). These values were obtained using a combination of the O_2 A-band with the weak CO_2/CH_4 absorption band at 1.61 µm and the strong CO_2 band at 2.06 µm. A spectral resolution of 0.04 nm (0.7 cm^{-1}), 0.075 nm (1.3 cm^{-1}) and 0.1 nm (1.73 cm^{-1}) for the O_2 A-band, the weak CO_2/CH_4 and the strong CO_2 band, respectively, were used with 2.5 spectral samples per FWHM and a SNR = 200. These studies show that the introduction of a multi-angle and multi-wavelength approach substantially improves the aerosol retrieval. The use

AMTD
8, 11853–11891, 2015

of a broader wavelength interval or other oxygen bands would further increase the information available at high spectral resolution.

The influence of the surface albedo on the retrieval has been evaluated by other groups as well, demonstrating that, at higher spectral resolutions, the information content is less dependent on the surface albedo (Corradini and Cervino, 2006). We found similar results in our surface albedo test, showing that at higher resolutions the absorption features are fully resolved, thus enhancing the aerosol contribution to the retrieval and reducing the contribution from surface reflectance.

It is a well understood fact that measurements at different wavelengths in the O_2 A-band are sensitive to different altitudes in the atmosphere. As a result, across the spectral window of the O_2 A-band, different wavelengths will penetrate to different depths in the atmosphere (Fig. 7). The wavelengths with the smallest absorption penetrate deepest into the atmosphere. Conversely, wavelengths with greater absorption are more sensitive to the upper parts of the atmosphere. Figure 2 shows that the spectral features are significantly degraded at low resolutions: the shape, depth and shoulder slope of the absorption bands are all changed. At a low resolution, much of the information coming from the spectral absorption features is lost; as a consequence, the information coming from different altitudes are mixed, resulting in a less resolved atmosphere. This effect also explains why the dependence of the reflected radiation from the surface on the retrieval is largest at lower resolutions. A less resolved absorption band results in an enhancement of the signal coming from the ground because the dynamic range of absorption optical thicknesses (and hence altitudes probed) is reduced. Consequently, the total amount of retrieved aerosol information increases with increasing spectral resolution, while the dependence on surface albedo decreases at the same time.

Many studies have pointed out that aerosol retrievals are strongly affected by noise (Geddes and Bösch, 2015; Hollstein and Fischer, 2014). In a sensitivity study based on a fast forward operator, Hollstein and Fischer (Hollstein and Fischer, 2014) investigates the aerosol information content at spectral resolution values of up to 0.01 nm ($0.17\,cm^{-1}$) and with a SNR ranging between 100 and 1000. Their simulations show

AMTD
8, 11853–11891, 2015

that aerosol optical depth retrievals benefit from an increase in the resolution (1 to 0.1 nm specifically); in comparison, aerosol height retrievals, could show a negative effect.

Geddes and Bösch (Geddes and Bösch, 2015) find a similar behavior in a study simulating aerosol retrievals among four different satellite-based instruments, GOSAT (Greenhouse Gases Observing Satellite), OCO-2 (Orbiting Carbon Observatory), Sentinel 5-P and CarbonSat, with spectral resolutions of 0.03 nm (0.52 cm^{-1}), 0.044 nm (0.76 cm^{-1}), 0.5 nm (8.65 cm^{-1}) and 0.1 nm (1.73 cm^{-1}), respectively. Using SNR of roughly < 200 (GOSAT), 400 (CarbonSat), 800 (OCO-2) and > 1000 (Sentinel-5 P) at 2×10^{20} photons s^{-1} m^{-2} sr^{-1} μm^{-1} they obtain DoF values between 4 and 5.

This comparison reveals that high instrument resolution does not necessarily lead to an improvement in the amount of information available, showing that the right combination of resolution and SNR is crucial for aerosol retrievals, and that a low resolution combined with a high SNR can lead to better results than a high resolution with a low SNR. However, their results also suggest that a combination of very high spectral resolution (> 0.03 nm) coupled with high SNR levels, leads to a larger amount of aerosol information (large values of DoF).

Our study generally reproduced the impact of SNR, as shown in the noise sensitivity tests, but the overall advantage of higher spectral resolutions on the information content dominated, i.e. it seems to be advantageous to use higher spectral resolution, even if this decreases SNR. We believe that this is due to the fact that the increased dynamic range of absorptions at higher spectral resolution, i.e., stronger line center absorptions at higher resolution (see Fig. 2), outweigh the decrease in SNR in the retrieval.

It should be noted that the pieces of information available depend on the noise model adopted and the way of sampling the high resolution spectra (in this study we have kept the ratio of FWHM and $\Delta\nu$ constant), which could impact the usefulness of higher resolution. However, all of the DoF determined in this study were calculated only for a portion of the O_2 A-band (13 122–13 140 cm^{-1}), representing the main molecular absorption feature, and not for the entire spectral range of the O_2 A-band. It is thus possi-

AMTD
8, 11853–11891, 2015

ble, although computationally expensive, to further improve the DoF when considering a larger spectra interval. More complex aerosol profiles, coupled with multi-angle simulations to improve the content of information, will be the subject of future research. Further, polarization can provide more information on the aerosol properties, and its impact on the retrieval needs to be investigated in more detail.

Our results give guidance for new satellite-based high resolution instruments for future satellite missions, such as the Panchromatic Fourier Transform Spectrometer (PanFTS) that is currently being developed to make geostationary measurements of atmospheric composition. In general, our results seem to indicate that improvements in the ability to retrieve aerosol height profiles can be achieved by sampling the O_2 A-band at high spectral resolution.

The Supplement related to this article is available online at doi:10.5194/amtd-8-11853-2015-supplement.

Acknowledgements. This work was funded by NASA's Jet Propulsion Laboratory through the Strategic University Research Partnership (SURP) program.

References

Anderson, B., Grant, W., Gregory, G., Browell, E., Collins, J., Sachse, G., Bagwell, D., Hudgins, C., Blake, D., and Blake, N.: Optical and microphysical characterization of biomass-burning and industrial-pollution aerosols from multiwavelength lidar and aircraft measurements, J. Geophys. Res., 107, 24117–24137, doi:10.1029/96JD00717, 1996. 11861

Ansmann, A., Althausen, D., Wandinger, U., Franke, K., Muller, D., Wagner, F., and Heintzenberg, J.: Vertical profiling of the Indian aerosol plume with six-wavelength lidar during INDOEX: a first case study, Geophys. Res. Lett., 27, 963–966, doi:10.1029/1999GL010902, 2000. 11861

AMTD
8, 11853–11891, 2015

Baidar, S., Oetjen, H., Coburn, S., Dix, B., Ortega, I., Sinreich, R., and Volkamer, R.: The CU Airborne MAX-DOAS instrument: vertical profiling of aerosol extinction and trace gases, Atmos. Meas. Tech., 6, 719–739, doi:10.5194/amt-6-719-2013, 2013. 11860, 11861

Blanchet, J. and List, R.: Estimation of optical properties of arctic haze using a numerical model, Atmos. Ocean, 21, 444–465, doi:10.1080/07055900.1983.9649179, 1983. 11861

Boesche, E., Stammes, P., Preusker, R., Bennartz, R., Knap, W., and Fischer, J.: Polarization of skylight in the O_2 A-band: effects of aerosol properties, Appl. Optics, 47, 3467–3480, doi:10.1364/AO.47.003467, 2008. 11856

Bovensmann, H., Burrows, J., Buchwitz, M., Frerick, J., Noël, S., Rozanov, V., Chance, K., and Goedec, A.: SCIAMACHY: mission objectives and measurement modes, J. Atmos. Sci., 56, 127–150, doi:10.1175/1520-0469(1999)056<0127:SMOAMM>2.0.CO;2, 1999. 11856

Clémer, K., Van Roozendael, M., Fayt, C., Hendrick, F., Hermans, C., Pinardi, G., Spurr, R., Wang, P., and De Mazière, M.: Multiple wavelength retrieval of tropospheric aerosol optical properties from MAXDOAS measurements in Beijing, Atmos. Meas. Tech., 3, 863–878, doi:10.5194/amt-3-863-2010, 2010. 11860, 11861

Corradini, S. and Cervino, M.: Aerosol extinction coefficient profile retrieval in the oxygen A-band considering multiple scattering atmosphere, test case: SCIAMACHY nadir simulated measurements, J. Quant. Spectrosc. Ra., 97, 354–380, doi:10.1016/j.jqsrt.2005.05.061, 2006. 11856, 11874, 11875

Crisp, D., Atlas, R., Breon, F.-M., Brown, L., Burrows, J., Ciais, P., Connor, B., Doney, S., Fung, I., Jacob, D., Miller, C., O'Brien, D., Pawson, S., Randerson, J., Rayner, P., Salawitch, R., Sander, S., Sen, B., Stephens, G., Tans, P., Toon, G., Wennberg, P., Wofsy, S., Yung, Y., Kuang, Z., Chudasama, B., Sprague, G., Weiss, B., Pollock, R., Kenyon, D., and Schroll, S.: The Orbiting Carbon Observatory (OCO) mission, Adv. Space Res., 34, 700–709, doi:10.1016/j.asr.2003.08.062, 2004. 11857

Deschamps, P., Breon, F.-M., Leroy, M., Podaire, A., Bricaud, A., Buriez, J.-C., and Seze, G.: The POLDER mission: instrument characteristics and scientific objectives, IEEE Geosci. Remote S., 32, 598–615, doi:10.1109/36.297978, 1994. 11856

Diner, D., Bruegge, C., Martonchik, J., Ackerman, T., Davies, R., Gerstl, S., Gordon, H., Sellers, P., Clark, J., Daniels, J., Danielson, E., Duval, V., Klaasen, K., Lilienthal, G., Nakamoto, D., Pagano, R., and Reilly, T.: MISR: a Multi-angle Imaging SpectroRadiometer for geophysical and climatological research from EOS, IEEE Geosci. Remote S., 27, 200–214, doi:10.1109/36.20299, 1989. 11856

AMTD
8, 11853–11891, 2015

Diner, D., Hodosa, R., Davisa, A., Garayb, M., Martonchika, J., Sanghavia, S., von Allmena, P., Kokhanovskyc, A., and Zhaid, P.: An optimization approach for aerosol retrievals using simulated MISR radiances, Atmos. Res., 116, 1–14, doi:10.1016/j.atmosres.2011.05.020, 2012. 11856

Dubovik, O., Holben, B., Eck, T., Smirnov, A., Kaufman, Y., King, M., Tanre, D., and Slutsker, I.: Variability of absorption and optical properties of key aerosol types observed in worldwide locations, J. Atmos. Sci., 59, 590–608, doi:10.1175/1520-0469(2002)059<0590:VOAAOP>2.0.CO;2, 2002. 11861

Dubuisson, P., Frouin, R., Dessailly, D., Duforêt, L., Leon, J.-F., Voss, K., and Antoine, D.: Estimating the altitude of aerosol plumes over the ocean from reflectance ratio measurements in the O_2 A-band, Remote Sens. Environ., 113, 1899–1911, doi:10.1016/j.rse.2009.04.018, 2009. 11856

Duforêt, L., Frouin, R., and Dubuisson, P.: Importance and estimation of aerosol vertical structure in satellite ocean-color remote sensing, Appl. Optics, 46, 1107–1119, doi:10.1364/AO.46.001107, 2007. 11856

Fischer, J. and Grassl, H.: Detection of cloud-top height from backscattered radiances within the oxygen A band. Part 1: Theoretical study, J. Appl. Meteorol., 30, 1245–1259, doi:10.1175/1520-0450(1991)030<1245:DOCTHF>2.0.CO;2, 1991. 11856

Frankenberg, C., Butz, A., and Toon, G.: Disentangling chlorophyll fluorescence from atmospheric scattering effects in O_2 A band spectra of reflected sunlight, Geophys. Res. Lett., 38, L03801, doi:10.1029/2010GL045896, 2011. 11857, 11858

Frankenberg, C., Hasekamp, O., O'Dell, C., Sanghavi, S., Butz, A., and Worden, J.: Aerosol information content analysis of multi-angle high spectral resolution measurements and its benefit for high accuracy greenhouse gas retrievals, Atmos. Meas. Tech., 5, 1809–1821, doi:10.5194/amt-5-1809-2012, 2012. 11857, 11874

Frieß, U., Sihler, H., Sander, R., Pohler, D., Yilmaz, S., and Platt, U.: The vertical distribution of BrO and aerosols in the Arctic: measurements by active and passive differential optical absorption spectroscopy, J. Geophys. Res., 116, D00R04, doi:10.1029/2011JD015938, 2011. 11861

Gabella, M., Kisselev, V., and Perona, G.: Retrieval of aerosol profile variations from reflected radiation in the oxygen absorption A band, Appl. Optics, 38, 3190–3195, doi:10.1364/AO.38.003190, 1999. 11856

AMTD
8, 11853–11891, 2015

Geddes, A. and Bösch, H.: Tropospheric aerosol profile information from high-resolution oxygen A-band measurements from space, Atmos. Meas. Tech., 8, 859–874, doi:10.5194/amt-8-859-2015, 2015. 11855, 11856, 11857, 11875, 11876

Hansen, J. and Lacis, A.: Sun and dust vs. greenhouse gases: an assessment their relative roles in global climate of change, Nature, 346, 713–719, doi:10.1038/346713a0, 1990. 11856

Hasekamp, O. and Landgraf, J.: Retrieval of aerosol properties over land surfaces: capabilities of multiple-viewing-angle intensity and polarization measurements, Appl. Optics, 46, 3332–3344, doi:10.1364/AO.46.003332, 2007. 11856

Heidinger, A. and Stephens, G.: Molecular line absorption in a scattering atmosphere. Part II: Application to remote sensing in the O_2 A band, J. Atmos. Sci., 57, 1615–1634, doi:10.1175/1520-0469(2000)057<1615:MLAIAS>2.0.CO;2, 2000. 11856

Hollstein, A. and Fischer, J.: Retrieving aerosol height from the oxygen A band: a fast forward operator and sensitivity study concerning spectral resolution, instrumental noise, and surface inhomogeneity, Atmos. Meas. Tech., 7, 1429–1441, doi:10.5194/amt-7-1429-2014, 2014. 11856, 11857, 11875

Johnson, B., Osborne, S., Haywood, J., and Harrison, M.: Aircraft measurements of biomass burning aerosol over West Africa during DABEX, J. Geophys. Res., 113, D00C06, doi:10.1029/2007JD009451, 2008. 11861

Kalashnikova, O. V., Garay, M. J., Martonchik, J. V., and Diner, D. J.: MISR Dark Water aerosol retrievals: operational algorithm sensitivity to particle non-sphericity, Atmos. Meas. Tech., 6, 2131–2154, doi:10.5194/amt-6-2131-2013, 2013. 11856

Koffi, B., Schulz, M., Breon, F., Griesfeller, J., Winker, D., Balkanski, Y., Bauer, S., Berntsen, T., Chin, M., Collins, W., Dentener, F., Diehl, T., Easter, R., Ghan, S., Ginoux, P., Gong, S., Horowitz, L., Iversen, T., Kirkevag, A., Koch, D., Krol, M., Myhre, G., Stier, P., and Takemura, T.: Application of the CALIOP layer product to evaluate the vertical distribution of aerosols estimated by global models: AeroCom phase I results, J. Geophys. Res., 117, D10201, doi:10.1029/2011JD016858, 2012. 11855

Kokhanovsky, A. and Rozanov, V.: The determination of dust cloud altitudes from a satellite using hyperspectral measurements in the gaseous absorption band, Int. J. Remote Sens., 31, 2729–2744, doi:10.1080/01431160903085644, 2010. 11856

Leiterer, U., Nagel, D., and Stolte, R.: Typical vertical profiles of aerosol spectral extinction coefficients derived from observations of direct solar radiation extinction during the aircraft exper-

AMTD
8, 11853–11891, 2015

iments Arctic Haze 94/95 and Merisec 93/94, Atmos. Res., 44, 73–88, doi:10.1016/S0169-8095(97)00010-0, 1997. 11861

Li, J., Scinocca, J., Lazare, M., Mcfarlaine, N., von Slazen, K., and Solheim, L.: Ocean surface albedo and its impact on radiation balance in climate models, J. Climate, 19, 6314–6333, doi:10.1175/JCLI3973.1, 2006. 11861

Martonchik, J., Kahn, R., and Diner, D.: Satellite Aerosol Remote Sensing over Land, Chapter 9: Retrieval of Aerosol Properties over Land using MISR Observations, edited by: Kokhanovsky, A. A. and De Leeuw, G., Springer, Berlin Heidelberg, doi:10.1007/978-3-540-69397-0_9, 267–293, 2009. 11856

Matsui, H., M. Koike, M., Kondo, Y., Takegawa, N., Fast, J., Pöschl, U., Garland, R., Andreae, M., Wiedensohler, A., Sugimoto, N., and Zhu, T.: Spatial and temporal variations of aerosols around Beijing in summer 2006: 2. Local and column aerosol optical properties, J. Geophys. Res., 115, D222, doi:10.1029/2010JD013895, 2010. 11861

Natraj, V., Jiang, X., Shia, R.-L., Huang, X., Margolis, J., and Yung, Y.: Application of principal component analysis to high spectral resolution radiative transfer: a case study of the O_2 A-band, J. Quant. Spectrosc. Ra., 95, 539–556, doi:10.1016/j.jqsrt.2004.12.024, 2005. 11856

Natraj, V., Spurr, R., Boesch, H., Jiang, Y., and Yung, Y.: Evaluation of errors from neglecting polarization in the forward modeling of O_2 A band measurements from space, with relevance to CO_2 column retrieval from polarization sensitive instruments, J. Quant. Spectrosc. Ra., 103, 245–259, doi:10.1016/j.jqsrt.2006.02.073, 2007. 11856

NOAA: U.S. Standard Atmosphere, U.S. Government Printing Office, Washington, D.C., 1976. 11860

Pelon, J., Mallet, M., Marisca, A., Goloub, P., Tanre, D., Bou Karam, D., Flamant, C., Haywood, J., Pospichal, B., and Victori, S.: Microlidar observations of biomass burning aerosol over Djougou (Benin) during African Monsoon Multidisciplinary Analysis Special Observation Period 0: Dust and Biomass-Burning Experiment, J. Geophys. Res., 113, D00C18, doi:10.1029/2008JD009976, 2008. 11861

Quinn, P., Coffman, D., Bates, T., Miller, T., Johnson, J., Welton, E., Neususs, C., Miller, M., and Sheridan, P.: Aerosol optical properties during INDOEX 1999: means, variability, and controlling factors, J. Geophys. Res., 107, D198020, doi:10.1029/2000JD000037, 2002. 11861

Rast, M., Bezy, J., and Bruzzi, S.: The ESA Medium Resolution Imaging Spectrometer MERIS: a review of the instrument and its mission, Int. J. Remote Sens., 20, 1681–1702, doi:10.1080/014311699212416, 1999. 11856

AMTD
8, 11853–11891, 2015

Rodgers, C.: Inverse method for atmospheric soundings – Theory and Practice, 13–79, World Scientific, Singapore, 2000. 11864

Rothman, L., Gordon, I., Barbe, A., Benner, D., Bernath, P., Birk, M., Boudon, V., Brown, L., Campargue, A., Champion, J.-P., Chance, K., Coudert, L., Dana, V., Devi, V., Fally, S., Flaud, J.-M., Gamache, R., Goldman, A., Jacquemart, D., Kleiner, I., Lacome, N., Lafferty, W., Mandin, J.-Y., Massie, S., Mikhailenko, S., Miller, C., Moazzen-Ahmadi, N., Naumenko, O., Nikitin, A., Orphal, J., Perevalov, V., Perrin, A., Predoi-Cross, A., Rinsland, C., Rotger, M., Simeckova, M., Smith, M., Sung, K., Tashkun, S., Tennyson, J., Toth, R., Vandaele, A., and Auwera, J. V.: The HITRAN 2008 molecular spectroscopic database, J. Quant. Spectrosc. Ra., 110, 533–572, doi:10.1016/j.jqsrt.2009.02.013, 2009. 11860

Rozanov, V. and Kokhanovsky, A.: Semianalytical cloud retrieval algorithm as applied to the cloud top altitude and the cloud geometrical thickness determination from top-of-atmosphere reflectance measurements in the oxygen A band, J. Geophys. Res., 109, D05202, doi:10.1029/2003JD004104, 2004. 11856

Samset, B. H., Myhre, G., Schulz, M., Balkanski, Y., Bauer, S., Berntsen, T. K., Bian, H., Bellouin, N., Diehl, T., Easter, R. C., Ghan, S. J., Iversen, T., Kinne, S., Kirkevåg, A., Lamarque, J.-F., Lin, G., Liu, X., Penner, J. E., Seland, Ø., Skeie, R. B., Stier, P., Takemura, T., Tsigaridis, K., and Zhang, K.: Black carbon vertical profiles strongly affect its radiative forcing uncertainty, Atmos. Chem. Phys., 13, 2423–2434, doi:10.5194/acp-13-2423-2013, 2013. 11855

Sanders, A. F. J. and de Haan, J. F.: Retrieval of aerosol parameters from the oxygen A band in the presence of chlorophyll fluorescence, Atmos. Meas. Tech., 6, 2725–2740, doi:10.5194/amt-6-2725-2013, 2013. 11856, 11857

Sanders, A. F. J., de Haan, J. F., Sneep, M., Apituley, A., Stammes, P., Vieitez, M. O., Tilstra, L. G., Tuinder, O. N. E., Koning, C. E., and Veefkind, J. P.: Evaluation of the operational Aerosol Layer Height retrieval algorithm for Sentinel-5 Precursor: application to O_2 A band observations from GOME-2A, Atmos. Meas. Tech. Discuss., 8, 6045–6118, doi:10.5194/amtd-8-6045-2015, 2015. 11856

Sanghavi, S., Martonchik, J. V., Landgraf, J., and Platt, U.: Retrieval of the optical depth and vertical distribution of particulate scatterers in the atmosphere using O_2 A- and B-band SCIAMACHY observations over Kanpur: a case study, Atmos. Meas. Tech., 5, 1099–1119, doi:10.5194/amt-5-1099-2012, 2012. 11856, 11857

AMTD
8, 11853–11891, 2015

Sayer, A. M., Smirnov, A., Hsu, N. C., Munchak, L. A., and Holben, B. N.: Estimating marine aerosol particle volume and number from Maritime Aerosol Network data, Atmos. Chem. Phys., 12, 8889–8909, doi:10.5194/acp-12-8889-2012, 2012. 11861

Schafer, J., Eck, T., Holben, B., Thornhill, K., Anderson, B., Sinyuk, A., Giles, D., Winstead, E., Ziemba, L., Beyersdorf, A., Kenny, P., Smirnov, A., and Slutsker, I.: Intercomparison of aerosol single-scattering albedo derived from AERONET surface radiometers and LARGE in situ aircraft profiles during the 2011 DRAGON-MD and DISCOVER-AQ experiments, J. Geophys. Res., 119, 7439–7452, doi:10.1002/2013JD021166, 2014. 11860

Shaw, G.: The Arctic Haze Phenomenon, Bullettin of the American Meteorological Society, 76, 2403–2413, doi:10.1175/1520-0477(1995)076<2403:TAHP>2.0.CO;2, 1995. 11861

Spurr, R.: VLIDORT: a linearized pseudo-spherical vector discrete ordinate radiative transfer code for forward model and retrieval studies in multilayer multiple scattering media, J. Quant. Spectrosc. Ra., 102, 316–342, doi:10.1016/j.jqsrt.2006.05.005, 2006. 11859, 11865

Tesche, M., Zieger, P., Rastak, N., Charlson, R. J., Glantz, P., Tunved, P., and Hansson, H.-C.: Reconciling aerosol light extinction measurements from spaceborne lidar observations and in situ measurements in the Arctic, Atmos. Chem. Phys., 14, 7869–7882, doi:10.5194/acp-14-7869-2014, 2014. 11861

Vuolo, M. R., Schulz, M., Balkanski, Y., and Takemura, T.: A new method for evaluating the impact of vertical distribution on aerosol radiative forcing in general circulation models, Atmos. Chem. Phys., 14, 877–897, doi:10.5194/acp-14-877-2014, 2014. 11855

Wagner, T., Beirle, S., Brauers, T., Deutschmann, T., Frieß, U., Hak, C., Halla, J. D., Heue, K. P., Junkermann, W., Li, X., Platt, U., and Pundt-Gruber, I.: Inversion of tropospheric profiles of aerosol extinction and HCHO and NO_2 mixing ratios from MAX-DOAS observations in Milano during the summer of 2003 and comparison with independent data sets, Atmos. Meas. Tech., 4, 2685–2715, doi:10.5194/amt-4-2685-2011, 2011. 11860

Wandinger, U., Müller, D., Bockmann, C., Althausen, D., Bosenberg, J., Weiss, V., Fiebig, M., Matthias, V., Wendisch, M., Stohl, A., and Ansmann, A.: Optical and microphysical characterization of biomass-burning and industrial-pollution aerosols from multiwavelength lidar and aircraft measurements, J. Geophys. Res., 107, 8125, doi:10.1029/2000JD000202, 2002. 11861

Xia, X., Chen, H., Wang, P., Zhang, W., Goloub, P., Chatenet, B., Eck, T., and Holben, B.: Variation of column-integrated aerosol properties in a Chinese urban region, J. Geophys. Res., 111, D05204, doi:10.1029/2005JD006203, 2006. 11861

AMTD
8, 11853–11891, 2015

Yamanouchi, T., Treffeisen, R., Herber, A., Shiobara, M., Yamagata, S., Hara, K., Sato, K., Yabuki, M., Tomikawa, Y., Rinke, A., Neuber, R., Schumachter, R., Kriews, M., Ström, J., Schrems, O., and Gernandt, H.: Arctic Study of Tropospheric Aerosol and Radiation (ASTAR) 2000: Arctic haze case study, Tellus, 57, 141–152, doi:10.1111/j.1600-0889.2005.00140.x, 2005. 11861

Yu, H., Chin, M., Winker, D. M., Omar, A., Liu, Z., Kittaka, C., and Diehl, T.: Global view of aerosol vertical distributions from CALIPSO lidar measurements and GOCART simulations: regional and seasonal variations, J. Geophys. Res., 115, D00H30, doi:10.1029/2009JD013364, 2010. 11861

Zarzycki, C. and Bond, T.: How much can the vertical distribution of black carbon affect its global direct radiative forcing?, Geophys. Res. Lett., 37, L20807, doi:10.1029/2010GL044555, 2010. 11856

Zhengjia, L., Shao, Q., TAO, J., and Chi, W.: Intra-annual variability of satellite observed surface albedo associated with typical land cover types in China, J. Geogr. Sci., 25, 35–44, doi:10.1007/s11442-015-1151-5, 2015. 11869

AMTD
8, 11853–11891, 2015

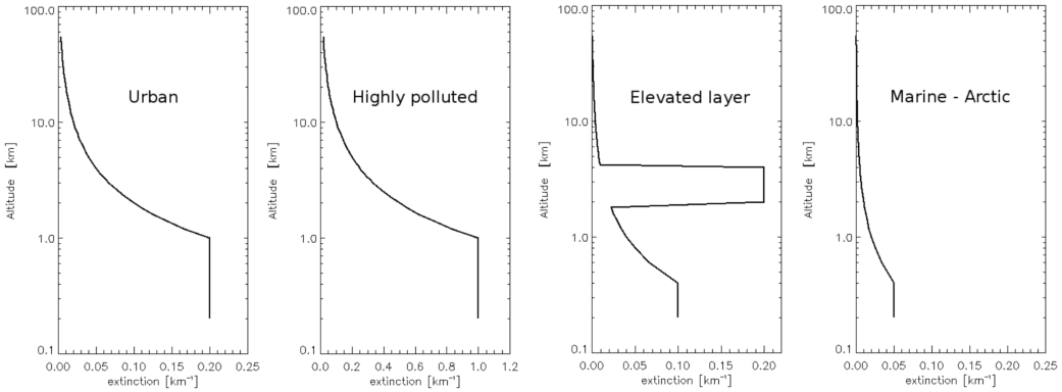

Figure 1. The four different aerosol profiles used in this study. From the left: urban ($k_{ext} = 0.2\,km^{-1}$, BLH = 1 km), highly polluted ($k_{ext} = 1\,km^{-1}$, BLH = 1 km), elevated layer ($k_{ext} = 0.2\,km^{-1}$, altitude range = 2–4 km), marine–arctic ($k_{ext} = 0.05\,km^{-1}$, BLH = 0.4 km).

AMTD
8, 11853–11891, 2015

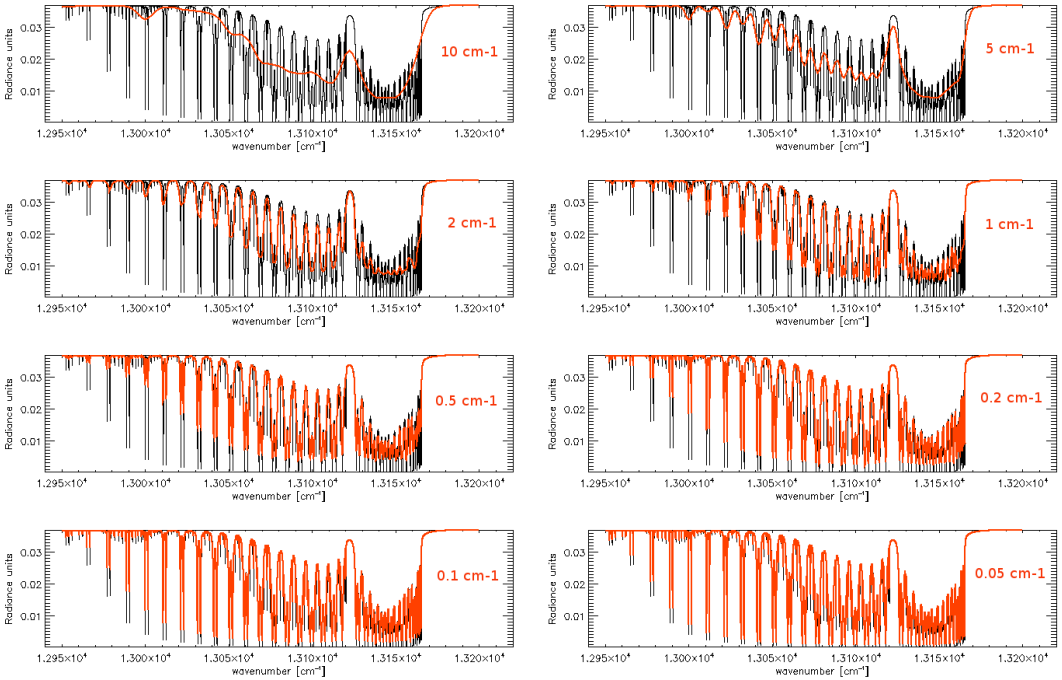

Figure 2. Example of O_2 A-band high resolution spectrum $\Delta\nu_0 = 0.002\,\mathrm{cm}^{-1}$ (black line) convolved with eight different instrument function FWHM (red line). For high resolution the narrow absorption features are well described, allowing a better retrieval of aerosol information.

AMTD
8, 11853–11891, 2015

A sensitivity study on the retrieval of aerosol vertical profiles using the oxygen A-band

S. F. Colosimo et al.

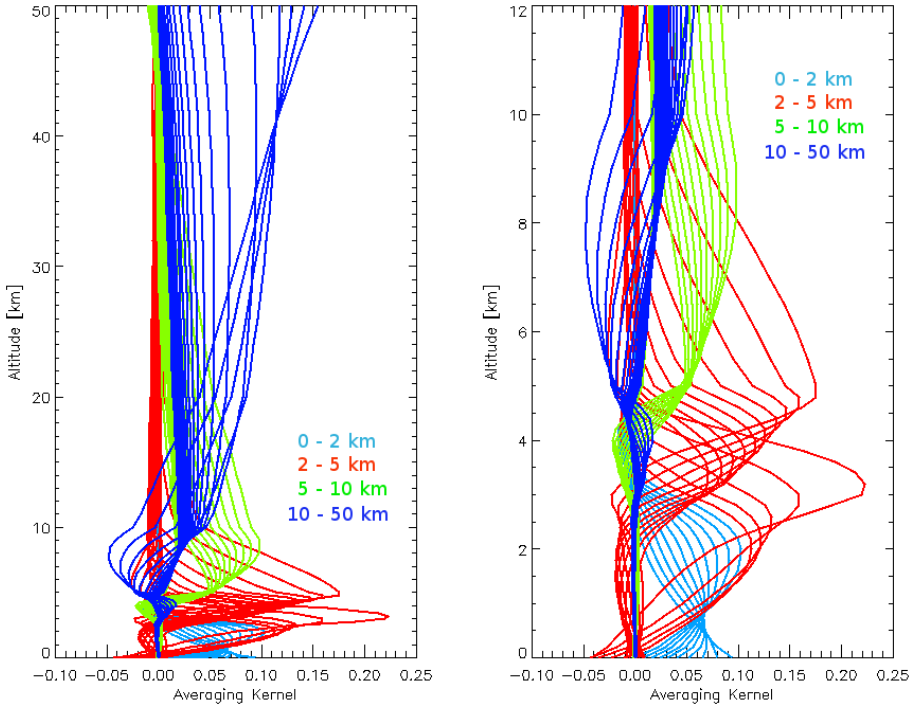

Figure 3. Example of averaging kernel vs. altitude. The simulation refers to a convolved spectrum of spectral resolution $\Delta\nu = 0.01\,\mathrm{cm}^{-1}$ and FWHM $= 0.05\,\mathrm{cm}^{-1}$ with a solar zenith angle SZA $= 45^{\circ}$ and an instrument viewing angle of 30° off-nadir. The AK are color coded for different altitude ranges. On the right, a zoom between 0 and 12 km is shown.

AMTD
8, 11853–11891, 2015

A sensitivity study on the retrieval of aerosol vertical profiles using the oxygen A-band

S. F. Colosimo et al.

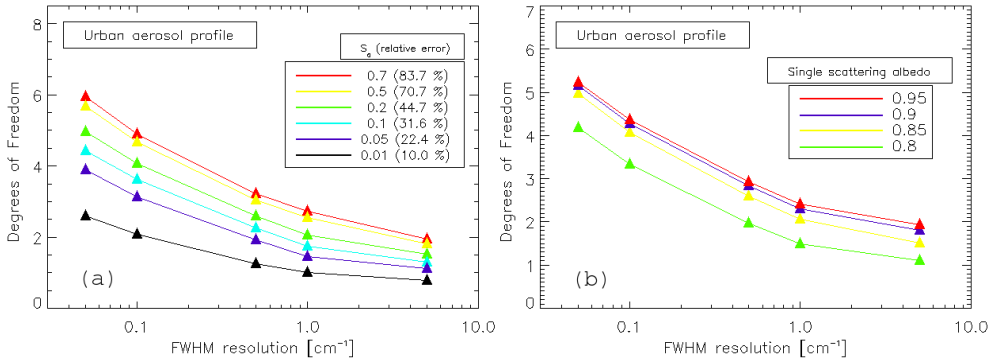

Figure 4. Urban scenario total Degrees of Freedom for different instrument resolution and different aerosol extinction profile uncertainties $\mathbf{S}_a$ **(a)**. Degrees of Freedom four values of single scattering albedo $\omega = [0.8, 0.85, 0.9, 0.95]$, to simulate different type of aerosol, are shown in **(b)**. A solar zenith angle SZA = 45° and a nadir instrument viewing have been used.

AMTD
8, 11853–11891, 2015

A sensitivity study on the retrieval of aerosol vertical profiles using the oxygen A-band

S. F. Colosimo et al.

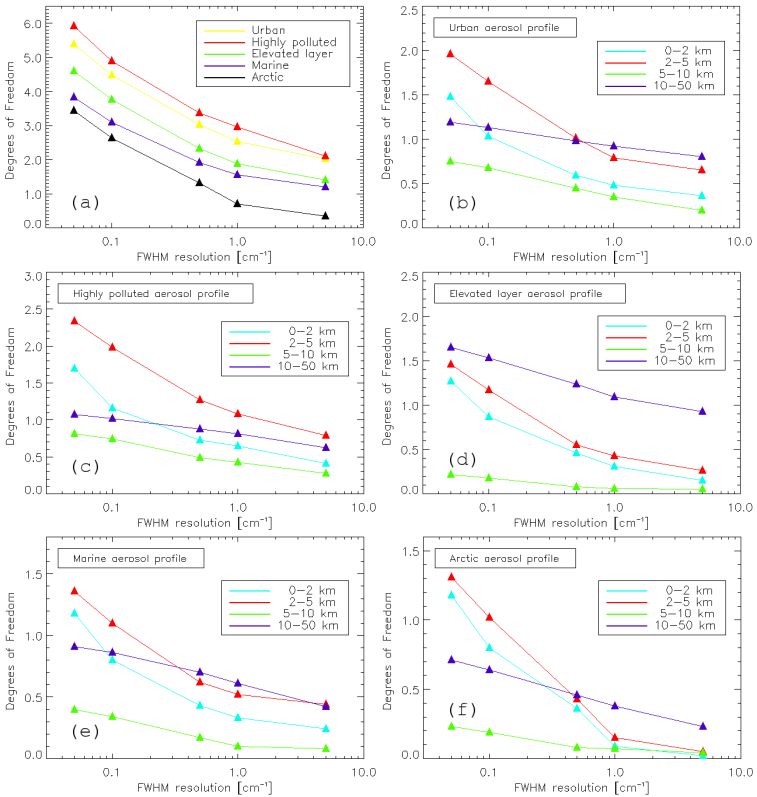

Figure 5. The DoF comparison for the different aerosol scenarios is shown in **(a)**. DoF calculated for four different altitude ranges to enhance the tropospheric contribution with respect to the whole atmosphere for every single aerosol scenario are shown in **(b–f)**. $\mathbf{S}_a = 0.2$ (44.7 % relative error) and $\omega = 0.95$ for the a priori aerosol extinction profile uncertainty and single scattering albedo are assumed. A solar zenith angle SZA = 45° and a 30° off-nadir instrument viewing geometry have been used in all the altitude tests.

AMTD
8, 11853–11891, 2015

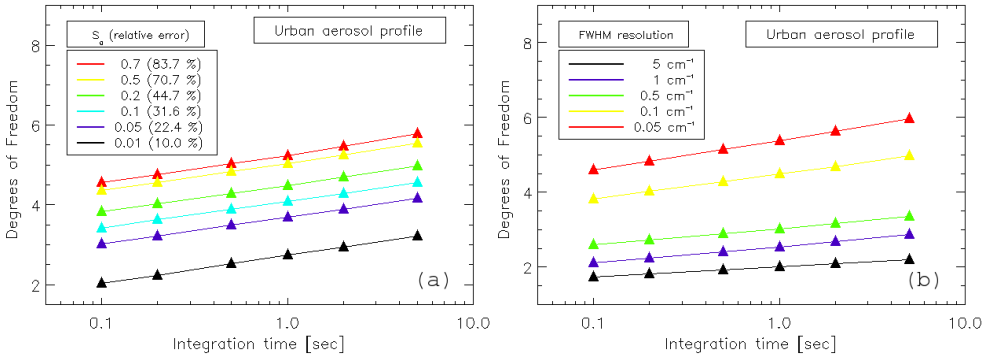

Figure 6. Integration time sensitivity for Urban scenario for different $\mathbf{S}_a$ **(a)** and different resolution **(b)**.

AMTD
8, 11853–11891, 2015

A sensitivity study on the retrieval of aerosol vertical profiles using the oxygen A-band

S. F. Colosimo et al.

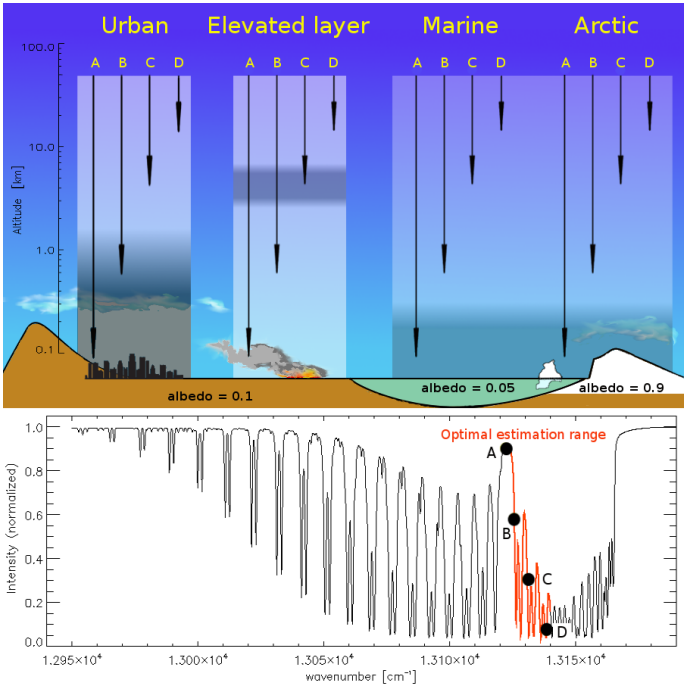

Figure 7. Example of how different instrument channels (different frequencies) probe different altitudes and thus different aerosol layers in the atmosphere. A generic channel A, sounding a spectral window of the oxygen A-band, penetrates more deeply in the atmosphere reaching the deeper levels because no absorption occurs. Moving along the shoulder of the band (channels B and C), the absorption process becomes more intense, preventing the radiation to penetrate deeper. At the bottom of the absorption band (channel D), the light is able to reach the upper part of the atmosphere only. This process is depicted in the sketch on top, where shaded gray areas represent the different aerosol profiles (arrows length is purely symbolic, not representing the actual altitude sounded at the corresponding channel).

AMTD
8, 11853–11891, 2015